Air quality changes during the COVID-19 lockdown over the Yangtze River Delta Region: An insight into the impact of human activity pattern changes on air pollution variation

Li Li [a,b,*], Qing Li [a,b], Ling Huang [a,b], Qian Wang [a,b], Ansheng Zhu [a,b], Jian Xu [a,b], Ziyi Liu [a,b], Hongli Li [a,b], Lishu Shi [a,b], Rui Li [a,b], Majid Azari [c], Yangjun Wang [a,b], Xiaojuan Zhang [a,b], Zhiqiang Liu [a,b], Yonghui Zhu [a,b], Kun Zhang [a,b], Shuhui Xue [a,b], Maggie Chel Gee Ooi [c,d], Dongping Zhang [a,b], Andy Chan [c,**]

[a] School of Environmental and Chemical Engineering, Shanghai University, Shanghai, 200444, China
[b] Key Laboratory of Organic Compound Pollution Control Engineering (MOE), Shanghai University, Shanghai 200444, China
[c] Department of Civil Engineering, University of Nottingham Malaysia, Semenyih 43500, Selangor, Malaysia
[d] Institute of Climate Change (IPI), National University of Malaysia (UKM), 43600 Bangi, Selangor, Malaysia

HIGHLIGHTS

- Air quality changes during the COVID-19 in YRD region are analyzed.
- The WRF-CAMx modelling system is applied to investigate impact of lowered human activities on air quality changes.
- Sources of the residual pollution are figured out for policy implications for future air pollution control.

GRAPHICAL ABSTRACT
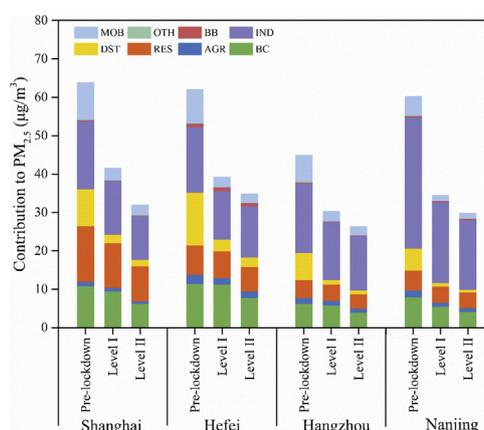
ARTICLE INFO

ABSTRACT

The outbreak of COVID-19 has spreaded rapidly across the world. To control the rapid dispersion of the virus, China has imposed national lockdown policies to practise social distancing. This has led to reduced human activities and hence primary air pollutant emissions, which caused improvement of air quality as a side-product. To investigate the air quality changes during the COVID-19 lockdown over the YRD Region, we apply the WRF-CAMx modelling system together with monitoring data to investigate the impact of human activity pattern changes on air quality. Results show that human activities were lowered significantly during the period: industrial operations, VKT, constructions in operation, etc. were significantly reduced, leading to lowered SO_2, NO_x, $PM_{2.5}$ and VOCs emissions by approximately 16–26%, 29–47%, 27–46% and 37–57% during the Level I and Level II response periods respectively. These emission reduction has played a significant role in the improvement of

* Correspondence to: L. Li, Key Laboratory of Organic Compound Pollution Control Engineering (MOE), Shanghai University, Shanghai 200444, China.
** Corresponding author.
E-mail addresses: Lily@shu.edu.cn (L. Li), Andy.Chan@nottingham.edu.my (A. Chan).

air quality. Concentrations of PM$_{2.5}$, NO$_2$ and SO$_2$ decreased by 31.8%, 45.1% and 20.4% during the Level I period; and 33.2%, 27.2% and 7.6% during the Level II period compared with 2019. However, ozone did not show any reduction and increased greatly. Our results also show that even during the lockdown, with primary emissions reduction of 15%–61%, the daily average PM$_{2.5}$ concentrations range between 15 and 79 μg m^{-3}, which shows that background and residual pollutions are still high. Source apportionment results indicate that the residual pollution of PM$_{2.5}$ comes from industry (32.2–61.1%), mobile (3.9–8.1%), dust (2.6–7.7%), residential sources (2.1–28.5%) in YRD and 14.0–28.6% contribution from long-range transport coming from northern China. This indicates that in spite of the extreme reductions in primary emissions, it cannot fully tackle the current air pollution. Re-organisation of the energy and industrial strategy together with trans-regional joint-control for a full long-term air pollution plan need to be further taken into account.

1. Introduction

At the end of the year 2019, the tragic coronavirus 2019 (COVID-19) pandemic occurred (Tian et al., 2020; Wang et al., 2020a) which has caused over 2.95 million global infections and 1931,000 deaths as of this writing (28th April 2020). Moreover the pandemic has caused enormorous economic and social disruption (Wang et al., 2020a). To control the rapid spread of the disease to protect people's health, China has enacted emergency response procedures, and required people to stay at home instead of going out beginning from late January 2020 (Tian et al., 2020; Wang et al., 2020b), resulting in significant reduction in the number of vehicle kilometres travelled (VKT), industrial operations, constructions, and even restaurants in operation, etc. Human and industrial activities were reduced to essential or bare minimal only. As we know that these are general emission sources that cause air pollution, especially during this particular winter season (Zhang et al., 2019). Thus the air quality during COVID-19 in China is much better than previous years in the same time period. The National Aeronautics and Space Administration (NASA) had published statellite imageries of the massive reduction in NO$_2$ over China resulting from the economic slow-down and the reduced human activities (NASA, 2020). Other analyses have similarly found that ground-based concentrations of key pollutants fell substantially across much of China (Wang et al., 2020a; Wang et al., 2020b).

Yangtze River Delta (YRD) region is one of the major economic city-clusters in Eastern China. The air pollution in the YRD region raises much attention (Huang et al., 2019; Li et al., 2018; Li et al., 2019), especially during winter, when the meteorological conditions are unfavourable, which usually cause more frequent air pollution episodes than other seaons. In this study, the air quality changes due to the lowered human activities during the COVID-19 are investigated to quantify the level of air quality improvement attributable to different aspects of human activities.

To understand the details of the air quality changes, we have divided the whole period into four stages: Pre-lockdown (1st January to 23rd January 2020); Level I response (roughly 24th January to 25th February 2020); Level II response (roughly 26th February to 31st March 2020) and Level III response (31st March onwards, 2020). The China's Spring Festival (Chinese New Year) is covered by Level I response period. According to the 'National Emergency Response Plan for Public Emergencies' issued by China State Council, the level of early warning is based on the degree of harm that may be caused by public emergencies, the degree of urgency and development. It is generally divided into four levels: Level I (particularly serious), Level II (serious), Level III (heavier) and Level IV (general). On 24th January 2020, the YRD region entered the first level of response, cities actively carried out epidemic prevention and control measures, including the adoption of compulsory measures in accordance with the law to stop all large-scale mass events such as bazaars and assemblies, etc. During Level I response period, the public significantly reduced the number of people and vehicles in public places, industrial enterprises, construction sites, catering enterprises

and other large-scale work stoppage and closure. After 2 months of struggle, the number of new confirmed cases per day across the country has dropped dramatically and more and more people are being cured and discharged from hospital. As the situation of the epidemic improved, on 25th February 2020, the emergency response level in Anhui and Jiangsu provinces was downgraded from a primary response to a secondary response. Zhejiang and Shanghai were adjusted on 2nd March and 24th March, respectively. Secondary response period, under the premise of good protective measures, the YRD cities allow some industrial enterprises to resume work and resume production, construction sites can be built; blanket cancellation of the village closures, citizens can rely on the health code and wear a mask to travel locally, road traffic flow gradually increased. Since 31st March, the YRD region enters into Level III period, with most activities gradually enetering into operation except schools, etc., of cause with strict protection measures. Here, we mainly foucus on the first three stages.

In this study, an integrated measurement-emission-modelling approach described in the next section including analysis of multi-pollutant observations, backward trajectory and potential source contribution analyses, estimates of pollutant emission reductions, and photochemical model simulations are adopted to conduct a comprehensive assessment of the impact of reduced human activity on air pollution reduction. We would like to achieve the following:

- To study the correlation between the substantial change of human and industrial activites on the air pollution scenarios in YRD: pre-lockdown, Level I response during lockdown, Level II response during lockdown;
- To study the changes of the source contributions to these air pollution scenarios which are related to local activity factors;
- To figure out sources of the residual pollution and investigate policy implications for future air pollution control.

2. Methodologies

To assess the effectiveness of the various emissions reductions linked with lowered human and industrial activities due to the COVID-19 restrictions, emission reductions associated with those limitations are calculated, and photochemical modelling is conducted to determine the changes in PM$_{2.5}$ attributed to specific emissions reductions.

2.1. Measurements

The hourly ambient mass concentrations of criteria air pollutants including SO$_2$, NO$_2$, CO, O$_3$, PM$_{2.5}$ and PM$_{10}$ are downloaded from the real time data published by the air monitoring data centre of Ministry of Ecology and Environment of the People's Republic of China (http://datacenter.mep.gov.cn). The meterological data are obtained from both National Oceanic and Atmospheric Administration (NOAA)'s

National Climate Data Center archive (http://www.ncdc.noaa.gov/oa/ncdc.html) and the National Data Center of the Chinese Meteorology Agency (http://data.cma.cn/).

2.2. Potential source contribution analysis

Potential source contribution factor (PSCF) analysis is applied in this study to locate pollution sources using air mass trajectories (Duan et al., 2019; Liu et al., 2019). It can be calculated for each $1° × 1°$ cell by dividing the number of trajectory endpoints corresponding to samples with factor scores or pollutant concentrations greater than specified values by the number of total endpoints in the cell (Hopke and Zeng, 1989;). Since the deviation of PSCF results can increase with the raise of distance between cell and receptor, a weight factor W_{ij} is adopted in this study to lower the uncertainty of PSCF results, named weighted PSCF (WPSCF; Hopke and Zeng, 1989; Polissar et al., 1999; Zhang et al., 2019). In this study, the TrajStat modelling system is used to analyse potential source contribution areas of $PM_{2.5}$ in Shanghai of YRD during different periods of the COVID-19 with the combination of Global Data Assimilation System (GDAS) meteorological data provided by the NCEP (National Center for Environmental Prediction). This shows us the air mass transport pathway during the three stages of lockdown.

2.3. Model setup

2.3.1. Model selection and parameter settings

In this study, the WRF-CAMx air quality numerical modelling system is used to evaluate the improvement in air quality resulting from the reductions of human activities during COVID-19. For the mesoscale meteorological field, we adopt the WRF model Version 3.4 (https://www.mmm.ucar.edu/wrf-model-general), and the CAMx model Version 6.1 (http://www.camx.com/). The gaseous and aerosol modules used in CAMx are the CB06 chemical mechanism (Yarwood et al., 2010) and CF module, respectively. The aqueous-phase chemistry is based on the updated mechanism of the Regional Acid Deposition Model (RADM) (Chang et al., 1987). The WRF meteorological modelling domain consists of three nested Lambert projection grids of 36 km - 12 km - 4 km, with 3 grids larger than the CAMx modelling domain at each boundary. WRF is run simultaneously for the three nested domains with two-way feedback between the parent and the nest grids. All the three domains utilise 27 vertical sigma layers with the top layer at

100 hPa. For the CAMx modelling domain shown in Fig. 1, we adopt a 36-12-4 km nested domain structure with 14 vertical layers, which are derived from the WRF 27 layers. The two outer domains cover much of Eastern Asia and Eastern China, respectively, while the innermost domain covers the YRD region. The simulation period is from 1st January to 31st March 2020, during which 1st to 5th January was utilised for model spin-up. We focus on three stages: Pre-lockdown (Jan 6 to Jan 24, 2020); Level I response (24th January to 25th February 2020) and Level II response (25th February to 31st March 2020) periods. We select four major cities including Shanghai, Nanjing, Hangzhou, and Hefei to study (shown in Fig. 1), which are capital cities of the provinces in the YRD region.

Initial and boundary conditions (IC/BCs) for the WRF modelling are based on $1° × 1°$ grids FNL Operational Global Analysis data that are archived at the GDAS. Boundary conditions to WRF are updated at 6-hour intervals for D01. The Yonsei University (YSU) scheme (Hong et al., 2006) is applied to parameterise the boundary layer processes; the NOAH land surface scheme (Ek et al., 2003) is used to describe the land-atmosphere interactions; the Purdue-Lin microphysics scheme (Lin et al., 1983) is chosen to reproduce the cloud and precipitation processes; the RRTM long-wave and Goddard Short-wave radiation schemes (Chou et al., 1999; Mlawer et al., 1997) are adopted to refect the radiation.

Anthropogenic source emission inventory for the YRD region is based on a most recent emission inventory developed by our group. Emissions for areas outside YRD in China is derived from the MEIC model (Multi-resolution Emission Inventory of China (http://www.meicmodel.org); anthropogenic emissions over other Asian regions are from the MIX emission inventory for 2010 (Li et al., 2017). Biogenic emissions are calculated by an updated version of the Model of Emissions of Gases and Aerosols from Nature (MEGAN, v3.0, http://aqrp.ceer.utexas.edu/projects.cfm). Sea salt emissions are simulated using the OCEANIC pre-processor developed by Ramboll (http://www.camx.com/download/support-software.aspx, last access on 17th April 2020). We further develop a reduced emission inventory to account for the restricted human activities due to COVID-19. Estimation of emission reductions for each source sector are based on reported acitivity data and our best estimates (see details in Section 3.4). The Sparse Matrix Operator Kernel Emissions (SMOKE, https://www.cmascenter.org/smoke, last access on 17th April 2020) model is used to process emissions into model needed format.
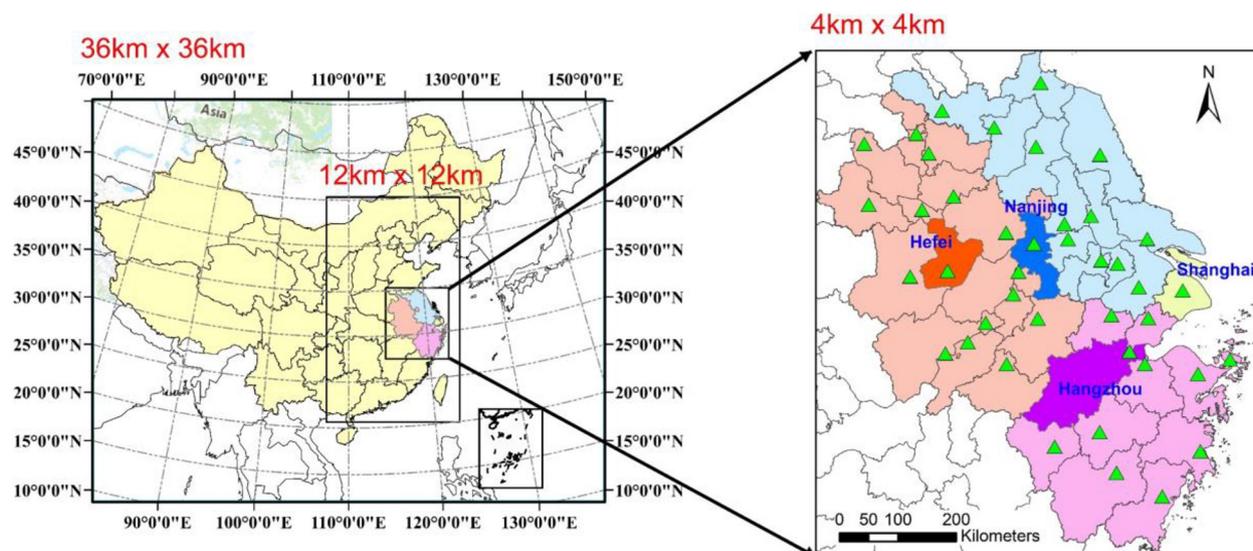
Fig. 1. Modelling domain and locations of the national observational sites (green triangle).

2.3.2. Model performance

Prior to evaluating the impact of the restricted human activities and thus the reduced emissions, the performance of the modelling system is evaluated to ensure to reasonably reproduce the observed meteorological conditions and air quality levels. Statistical indices used for WRF model evaluation include Mean Bias (MB), Correlation Coefficient (R) and Root Mean Square Error (RMSE). Table 1 shows the summary statistics for the comparisons of main meteorological parameters simulated by the WRF model with observed data. Figs. S1(a) to (d) show the comparisons of hourly simulations of 2 m surface temperature, 10 m wind speed, relative humidity and pressure at capital cities (Shanghai, Hangzhou, Nanjing, Hefei) in the YRD region with observed data. The observational data are abstracted from the airport observational data from NOAA's National Climate Data Center archive (http://www.ncdc.noaa.gov/oa/ncdc.html). It can be shown that the temperature simulations are very good, including the trend and local maxima and minima in the entire simulation period with R value of over 0.83. This is consistent with many other works where thermal fluxes are accurately captured. Simulations of the wind speed also achieve reasonably good correlation (0.53–0.64). On the other hand, the agreement between observed and predicted humidity data are generally low, with negative mean bias. Overall, the model performances are consistent with observed data.

In terms of CAMx model perforamcne evaluation, we presented mean bias (MB), normalized mean bias (NMB), fractional bias (FB) and fractional error (FE) of PM$_{2.5}$ at 41 monitoring sites over the YRD region during our simulatin period (Table S1). FB and FE values for 39 out of 41 monitoring sites fall within the standards recommended by EPA (EPA 2007), indicating acceptable model performance for PM$_{2.5}$. Fig. 2 further shows the scatter plots of observed and simulated averaged PM$_{2.5}$ concentrations during pre-lockdown, Level I and Level II preiods. Results show the model is overall underpredicting PM$_{2.5}$ concentrations and slightly better agreement is observed for during pre-lockdown period than lockdown periods. Due to large uncertainties associated with the estimation of emission reductions during lockdown, therefore, we used the concept of relative response factor to quantify the impact of emission reductions on air quality changes to reduce model uncertainties.

2.3.3. Method for quantifying the impact of lowered human activity on air quality

Quantifying the air quality changes in response to lowered human activities and the resulting emission reductions was done using the so called Brute Force Method (BFM) (Burr and Zhang, 2011), where a baseline scenario is simulated using unadjusted emissions (i.e. those

Fig. 2. Scatter plots of observed and simulated PM$_{2.5}$ concentrations during pre-lockdown, Level I and Level II response periods at 41 monitoring sites over the YRD region (locations are monitoring sites shown in Fig. 2).

emissions that would have occurred in absence of the COVID-19) and a reduction scenario is modelled based on the emission reductions estimation (See details in Section 3.4). For emission reductions outside the YRD region during lockdown, we apply the reduction ratio used by Wang et al. (2020b). In both cases, the same meteorology are utilised to drive the photochemical model simulations. Through a comparative analysis of the scenarios, a relative improvement factor RF for a given atmospheric pollutant, resulting from emission reductions, can be calculated and combined with ground based observations to assess the changes in air quality associated with those emission reductions caused due to lowered human activities,

$$RF = (C_b - C_s)/C_b \tag{1}$$

$$C_d = C_o \cdot RF \tag{2}$$

where C_b is the simulated pollutant concentration in the base case (μg m^{-3}), C_s is the pollutant concentration in the COVID-19 scenario (μg m^{-3}), C_o denotes the actual observed concentration at the site (μg m^{-3}) and C_d is the concentration reduction caused by the emissions reduction (μg m^{-3}). We calculate the relative improvement factor (RF) for Level I and Level II periods, separately. These factors are applied at selected monitoring sites to reflect the changes of air quality associated with COVID-19 induced emission reductions.

The Particulate Source Apportionment Technology (PSAT) coupled in the CAMx is utilised to quantify the sectoral contributions to PM$_{2.5}$ from eight source categories (aggregated from detailed source sectors listed in Table S2) under both baseline and COVID-19 scenarios. These eight source categories are industrial (IND, including industrial boiler, kiln, power plants, industrial processes), mobile (MOB, including onroad, offroad machinery, aircraft), agricultural (AGR), residential (RES, including cooking, residential combustion, waste treatment), dust (DST, including construction dust and road dust), biomass burning (BB), other anthropogenic (OTH, e.g. autorepair, building paints, gas station, hospital, etc.), and natural (NAT, including biogenic emissions and seasalt emissions). Differences in PSAT results under baseline and COVID-19 scenarios are used to quantify the contributions of PM$_{2.5}$ reductions associated with emissions reduction in individual sectors due to the lowered human activities.

Table 1
Statistical evaluation of WRF model performance during COVID-19 (2020/1/1–2020/3/31).

Parameters	Site	Sim	Obs	MB	RMSE	R
T$_2$ (°C)	SH	7.9	9.2	−1.2	2.7	0.83
	HZ	9.3	9.7	−0.3	2.6	0.86
	NJ	6.8	7.9	−1.1	2.9	0.86
	HF	6.7	7.4	−0.6	3.3	0.83
	NB	8.9	9.8	−0.8	2.9	0.84
	Avg	7.9	8.8	−0.8	2.9	0.84
WS$_{10}$ (ms^{-1})	SH	4.4	4.8	−0.4	1.8	0.64
	HZ	3.1	2.5	0.6	1.6	0.62
	NJ	3.6	2.6	1.0	1.9	0.53
	HF	3.4	3.0	0.4	1.6	0.58
	NB	3.7	2.8	0.9	2.0	0.63
	Avg	3.6	3.1	0.5	1.8	0.60
RH(%)	SH	75.2	75.8	0.1	12.9	0.78
	HZ	65.4	76.2	−10.2	17.6	0.76
	NJ	70.3	78.3	−7.3	17.3	0.75
	HF	68.6	79.5	−10.1	19.6	0.72
	NB	74.9	77.1	−1.2	14.4	0.76
	Avg	70.9	77.4	−5.8	16.4	0.75

Table 2
Changes of meterological parameters at typical cities in the YRD region.

Site	2017–2019(1/1-3-31)			2020(1/1-3-31)	2017–2019(1/1-3-31)			2020(1/1-3-31)
	Avg ± Std	Max	Min	Avg ± Std	Avg ± Stdev	Max	Min	Avg ± Std
Temperature/°C					Pressure/hPa			
Shanghai	7.9 ± 4.3	10.6	5.3	9.7 ± 4.2	1024.7 ± 5.8	1028.8	1020.5	1023.8 ± 5.6
Hangzhou	8.6 ± 5.1	11.8	5.6	10.2 ± 5.0	1024.2 ± 5.9	1028.4	1020	1023.4 ± 5.7
Nanjing	6.9 ± 5.7	10.1	3.7	8.5 ± 5.4	1024.6 ± 6.2	1029	1020.2	1023.7 ± 6.1
Hefei	6.8 ± 6.0	10.1	3.5	8.1 ± 5.8	1024.2 ± 6.4	1028.6	1019.6	1022.7 ± 5.8
Wind speed/m·s^{-1}					Relative humidity/%			
Shanghai	4.8 ± 2.1	6.5	3.2	4.9 ± 2.0	74.8 ± 17.6	87.8	61.5	75.7 ± 16.8
Hangzhou	2.7 ± 1.4	3.9	1.7	2.5 ± 1.5	75.6 ± 19.4	90	60.6	76.4 ± 18.4
Nanjing	2.7 ± 1.6	4	1.5	2.6 ± 1.6	74.8 ± 20.6	88.6	61.3	78.3 ± 21.7
Hefei	3.0 ± 1.6	4.3	1.9	3.1 ± 1.6	74.1 ± 20.5	88.9	59.2	79.2 ± 21.6
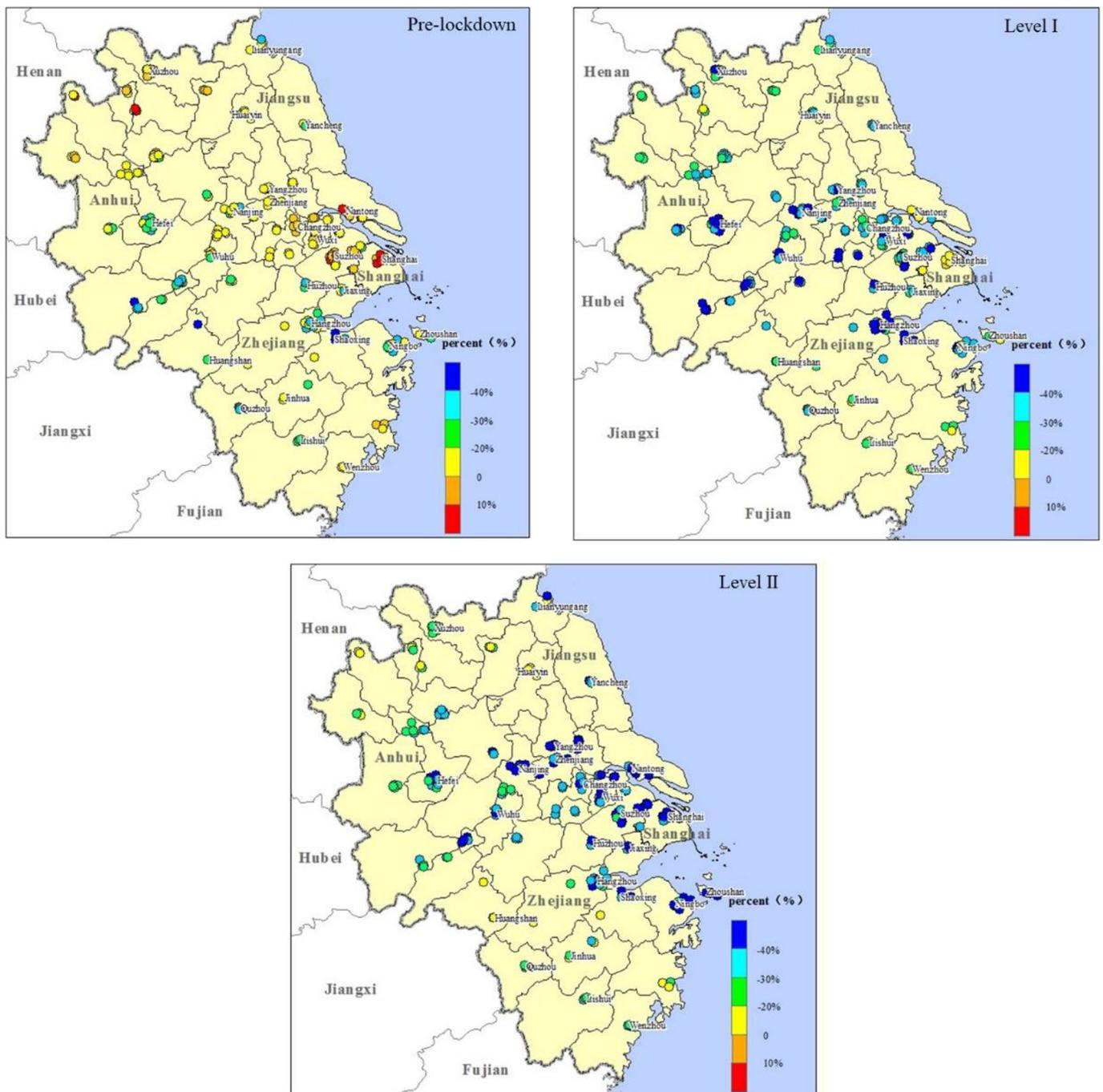
Fig. 3. Relative changes of PM$_{2.5}$ during Pre-lockdown, Level I and Level II periods in YRD.

3. Results and discussions

3.1. Meteorological changes during the COVID-19 period compared with previous years

We compare the hourly meteorological data of Shanghai, Hangzhou, Nanjing and Hefei during January to March from 2017 to 2020, results are shown in Table 2. As indicated in Fig. S2 and S3, on the whole, there is no obvious change during COVID-19 in terms of air pressure, temperature and wind field from January to March 2020 compared with previous years, except that the surface temperature during Jan and Feb is somehow higher than previous years.

3.2. Air quality changes before and during the COVID-19 period

Fig. 3 shows the changed concentration of $PM_{2.5}$ before the lockdown, Level I response and Level II response periods, respectively. From the angle of $PM_{2.5}$, almost all the cities show obvious reduction during Level I and Level II, especially in the central area of YRD where the vehicle populations are high. From Fig. S4, it can be shown that NO_2 reduced sharply, especially during Level I period over the YRD reigon, decrease ratio of SO_2 is much lower than NO_2, while O_3 rebuced almost all over the YRD region. In general, the level of $PM_{2.5}$ is fairly low over the entire YRD region, classified internationally at good air quality level, as is shown in Fig. S4.

As shown in Fig. 4, the average concentrations of criteria pollutants at 41 cities in the YRD region from January to March 2020 (except for the rebound of O_3-8h) are much lower compared with 2017–2019 in the same periods of Pre-lockdown, Level I response, and Level II response. Concentrations of $PM_{2.5}$, PM_{10}, CO, NO_2 and SO_2 decreased by 12.3%, 19.6%, 7.8%, 18.5% and 29.3% compared with 2019 before the epidemic, and 31.8%, 33.7% and 20% 9%, 45.1% and 20.4% reduction respectively during the first-level response period, decrease of 33.2%, 29.0%, 14.7%, 25.9%, 27.2% and 7.6% in the Level II response period. During the Level I response period, NO_2 sharply decreased by 45.1%, but O_3-8h rebound was the most obvious, the increasing rate was 20.5%.

From Fig. S5, Table S3 and Table S4, it can be shown that concentrations of $PM_{2.5}$, PM_{10}, CO, NO_2 and SO_2 decrease most significantly during Level I period, followed by Level II response period. This indicates that during the lockdown, the stoppage of industrial activities in various enterprises, construction sites, eateries have produced conspicuous results in air pollution reduction. In particular, during Level I period, Zhejiang, Anhui and Jiangsu has more pronounced air quality improvement compared to Shanghai, suggesting that the response from each provinces have slightly different level of implementation of lockdown. Moreover the drop of NO_2 is most prominent, e.g. Zhejiang (51.7%), Jiangsu (44.7%), Anhui (42.8%) and Shanghai (29.5%) respectively, which is related to the sharp decrease of VKT and the closed mid and small enterprises. On the other hand, the rebound of 8-h O_3 during the first-level response is similarly significant: Zhejiang is the highest, followed by Anhui, Shanghai and Jiangsu with an increase of 28.7%, 22.7%, 16.2% and 12.4% respectively. This can be attributed to the fact that during the lockdown, there are a large reduction of industrial activities and vehicular traffic leading to a sharp drop of NO_x (−29.5% to −51.7%), while the amount drop of VOC is not as large as NO_x, leading to a drop in titration effect towards ozone. Further policies regarding reducing regional atmospheric oxidation capacity is in urgent need to takle the increasing ozone issue in the region.
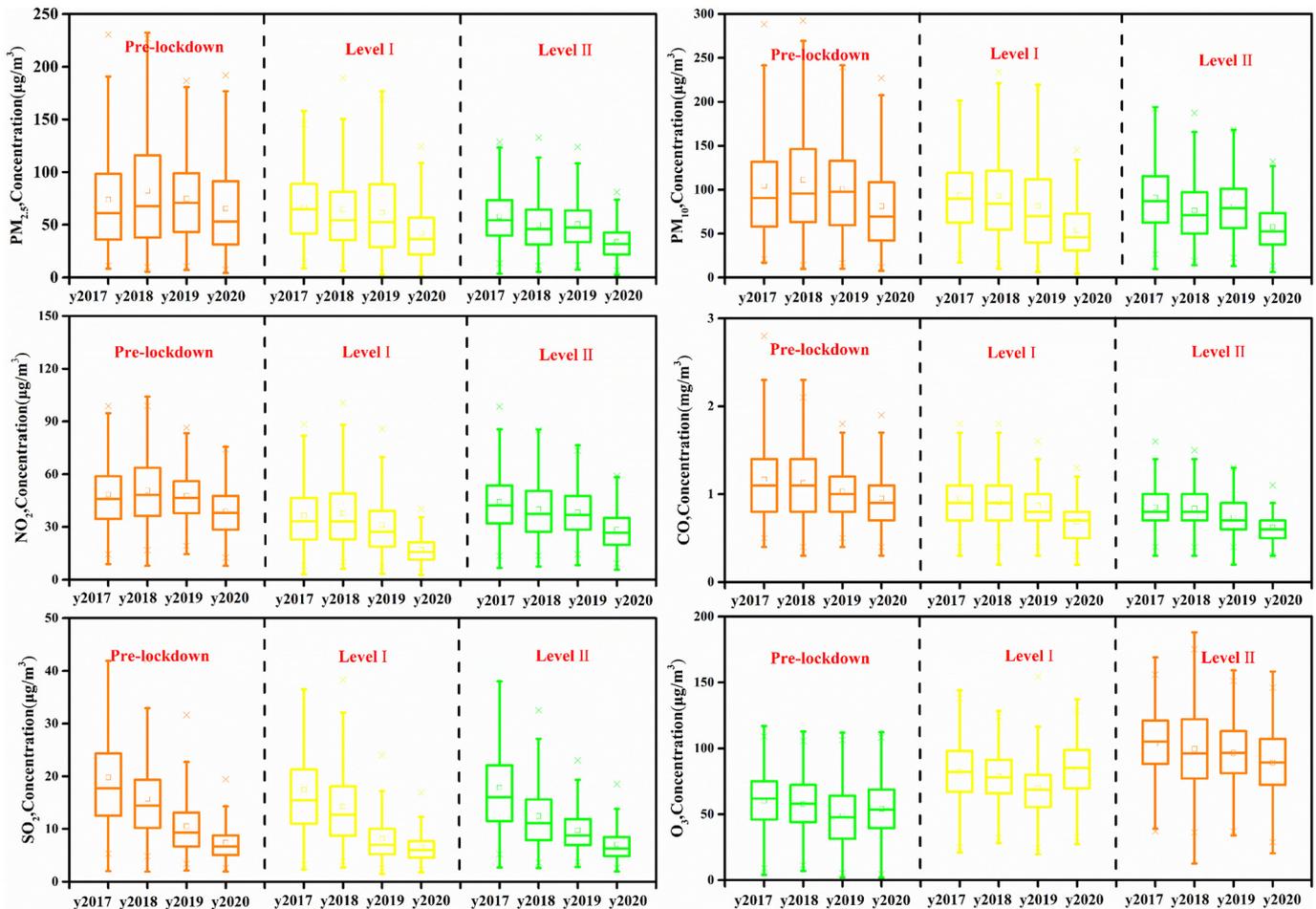
Fig. 4. Yearly changes of $PM_{2.5}$, PM_{10}, CO, NO_2, SO_2 and O_3-8h in 41 cities in the YRD during 1st January - 31st Mar, 2020.

3.3. Clustering analysis and potential source contributions

To further study the air mass trajectories and source characteristics of $PM_{2.5}$ in the YRD during the three stages, PSCF is used to qualitatively analyse the source regions of $PM_{2.5}$ pollution. The PSCF threshold of $PM_{2.5}$ is set to be 75 μg m^{-3}, which is in line with the daily average standard. Fig. 5 shows the results of potential source contribution factors. The darker the grid colour, the greater contribution of the potential source area to the $PM_{2.5}$ concentration in Shanghai. Overall, the potential contribution areas of $PM_{2.5}$ affecting Shanghai are widely distributed and the sources of pollution are complicated. They are mainly concentrated in Anhui, Jiangsu, Zhejiang, Shandong, Henan, Shanxi, Hebei, and Shanghai. Jiangxi, Hunan, Beijing, Tianjin, Hebei, and other regions. There is also a minor contribution from the surrounding area. It can be seen that Shanghai is not only affected by local and nearby cities in the YRD region, but also affected by long-range transport as well.

Before the epidemic and during Level I response, the potential impact source areas of Shanghai mainly include three categories: 1) The local potential source areas are mainly from where the recipient city is adjacent to the neighbouring area, and are distributed in the North and Northwest of the Shanghai (Xuzhou-Suzhou-Wuxi-Changzhou-Nantong area), its WPSCF is above 0.6; 2). The regional potential sources are located in the southwest and southern cities of the recipient city, mainly including the impact of the northern cities of Zhejiang Province, Huzhou and Jiaxing, with the WPSCF is above 0.5; 3). The potential sources are located in Jiangsu. In the eastern coastal area, the polluted air mass mainly comes from the north. It is influenced by the northeast trade winds and the coast current from north to south. The polluted air

mass landed in Shanghai after detouring at sea, and the WPSCF was 0.3–0.4.

During the Level II period, the WPSCF results show that Shanghai is mainly affected by the contribution of cities in the region. The regional potential source is located in the southwestern city of the recipient city, mainly including Huzhou, a city in the north of Zhejiang Province, and the WPSCF is above 0.6. YRD is located in the monsoon area, affected by the monsoon climate since March, it is natural that Shanghai receives more southerly winds (southeast and southwesterly winds), which has caused polluted air masses. Industries have resumed production, and economic activities have brought more man-made sources after Level II response.

Figs. S6 and Table S5 shows the air mass trajectories of Pre-lockdown-C1, and indicate their sources are similar. The air masses originate from Northern Mongolia and Siberia, and reaches the YRD region after passing through Beijing, Tianjin and Yellow Sea region. Through this air mass, it is shown that at all periods in 2019, the concentration of CO and $PM_{2.5}$ is higher. This shows that this air mass carried primary and secondary air pollutants through long distances. This indicates that in winter season, more large scale regional joint-control is necessary.

3.4. Emissions reduction estimation during the COVID-19

It is important to realise the lockdown coincided with the Chinese New Year (CNY) holidays, which officially began on the 25th January 2020. It is traditional that many industries and commercial activities will slow down two or three days before the CNY holidays, labour-intensive industries take holidays even earlier, which will last until a
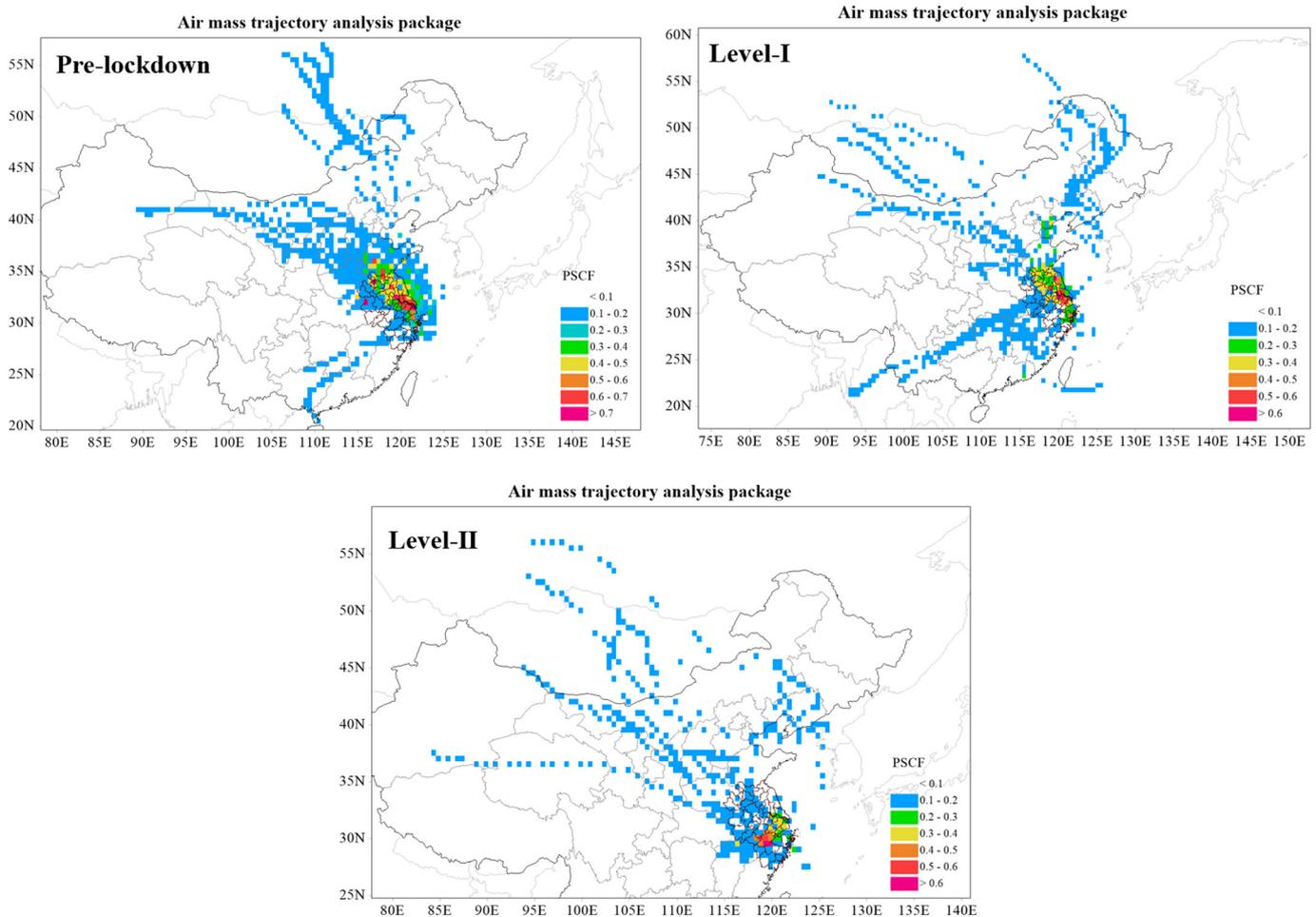
Fig. 5. $PM_{2.5}$ potential source regions: air mass trajectory analysis during different stages in Shanghai.

Table 3
Emission reduction estimations for various emission source sectors.

		Level I response period						Level II response period					
		SO$_2$	NO$_x$	CO	VOCs	PM$_{10}$	PM$_{2.5}$	SO2	NOx	CO	VOCs	PM10	PM2.5
Industry	Stationary source	−34%	−20%	−38%	−32%	−29%	−29%	−19%	−12%	−22%	−21%	−18%	−18%
	Industrial processing	−33%	−29%	−32%	−51%	−36%	−36%	−19%	−18%	−23%	−28%	−19%	−19%
Mobile	Vehicle exhause	−75%	−75%	−75%	−75%	−75%	−75%	−50%	−50%	−50%	−50%	−50%	−50%
	Non-road	−90%	−90%	−90%	−90%	−90%	−90%	−50%	−50%	−50%	−50%	−50%	−50%
	Aircraft	−80%	−80%	−80%	−80%	−80%	−80%	−60%	−60%	−60%	−60%	−60%	−60%
Dust	Construction dust					−90%	−90%					−50%	−50%
	Road dust					−75%	−75%					−50%	−50%
Solvent usuage	Dry cleaning				−100%						−100%		
	Vehicle repair				−100%						−100%		
	Architectural Coating				−100%						−100%		
	Household solvent usage				30%						10%		
	Hosipital solvent usage				30%						10%		
Storage	Gas station				−50%						−30%		
	Oil storage				−50%						−30%		
Cooking					−90%	−90%	−90%				−90%	−90%	−90%
Residential combustion		10%	10%	10%	10%	10%	10%	0%	0%	0%	0%	0%	0%
Biomass burning		10%	10%	10%	10%	10%	10%	0%	0%	0%	0%	0%	0%
Total emission reduction ratio		−26%	−47%	−39%	−57%	−61%	−46%	−15%	−29%	−25%	−37%	−36%	−27%

week after the CNY. Meanwhile, migrant workers return home and people start to visit friends and relatives. However, most people choose to stay at home during this CNY, which is the biggest difference from the holiday in previous years. Thus, the Spring Festival in 2020 is almost covered by the Level I response period.

Officially, the YRD cities started its full lockdown on January 23rd - 25th and remained in place until the end of February. In the meantime, the production activities of industries and pollutant emissions are not exactly at full capacity due to the seriousness of the COVID-19 epidemic.

During the full lockdown, almost all medium and small industries except power plants and large-scale enterprises were closed. We attempt to analyse the activity levels of each respective sector. Power production and demand was subsequently significantly reduced as a result of decline in demand. According to published official data by Anhui (Anhui Provincial Bureau of Statistics, http://tjj.ah.gov.cn/) and Jiangsu (JiangSu Energy Regulatory Office of National Energy Administration

of the People's Republic of China, http://jsb.nea.gov.cn/) provinces, cumulative electricity generation in Anhui and Jiangsu provinces fell by 19% and 18% in January–February 2020 compared to the same period in 2019, with the decline in February reaching 27% and 26%, respectively. The manufacturing sector did not actually show major slowdown: according to the industrial production data published by the bureau of statistics in the provinces of the YRD, the production of iron and other non-ferrous materials, medical and pharamaceutical remained roughly constant. The petrochemical industry, construction industry, facility manufacturing were strongly affected and hampered by both the upstream and downstream chain. All other industries were almost brought to a standstill as a result of these supply chain movements. The impact of the COVID-19 epidemic on industrial production can be seen in the sharp decline of 29% and 32% in industrial electricity consumption in January–February 2020 in Anhui and Zhejiang provinces.
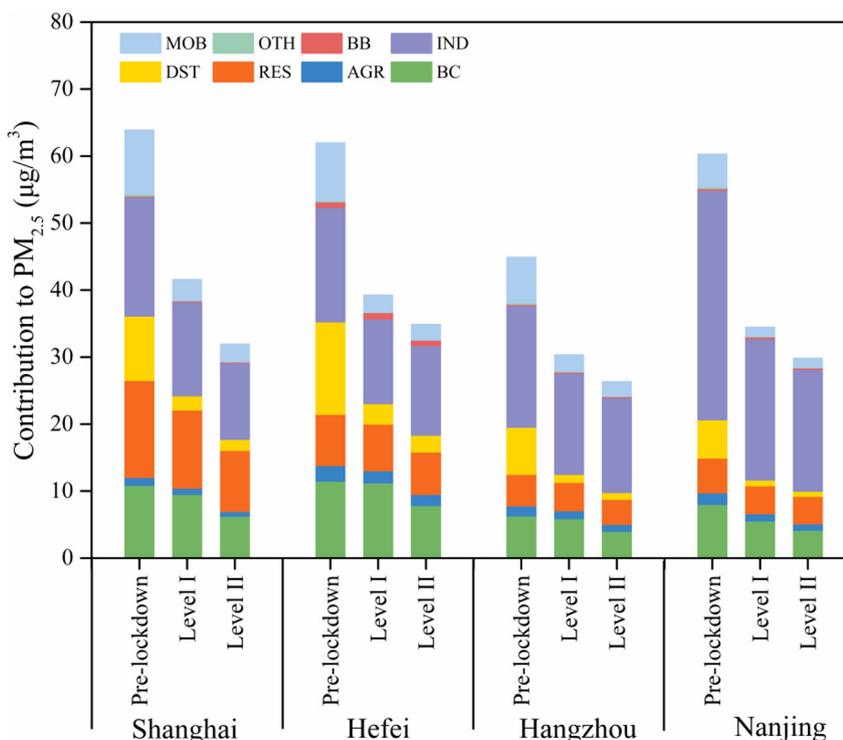
Fig. 6. Source contribuitons to PM$_{2.5}$ at Shanghai, Hefei, Hangzhou and Nanjing during pre-lockdown, Level I and Level II response periods.

In the non-industrial sectors, citizens were at a restricted movement order and they could not go out to the streets, leading to a sharp decline in vehicle and public transport. Data published by the bureau of statistics of Anhui and Zhejiang provinces showed that passenger traffic in both provinces dropped significantly by 50% in January–February 2020 compared to the same period in 2019. While traffic flow monitoring data from Bengbu and Changzhou cities showed a 75% decline in the first-level response period and a 50% decline during the second-level
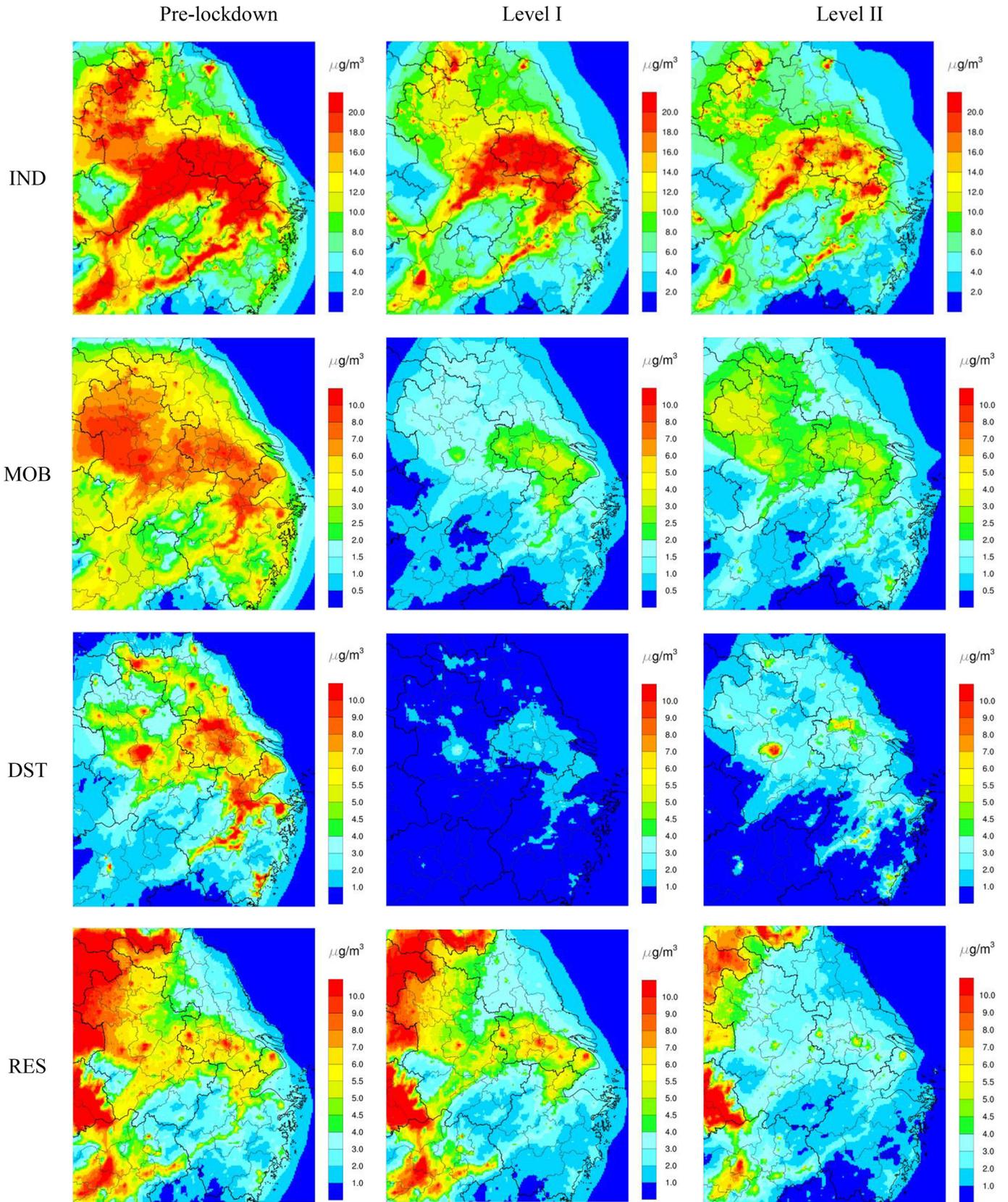
Fig. 7. Sectoral contribuitons to PM$_{2.5}$ during pre-lockdown, Level I and Level II response periods in YRD.

response period, compared to pre-epidemic period. As to the total departures from China's 25 busiest airports (Flightradar 24, https://www.flightradar24.com/), the decline ratio is 80% and 60%, respectively. The construction and service industry came to almost a total halt: restaurants, construction sites, laundries, automobile service, renovation and refurbishment were all stopped proactively or involuntarily. It is interesting to know that during the epidemic, there is an observable increase in the use of solvents and volatile organic compound domestically and in the hospital, plus a small increase in domestic combustion and biomass burning during the first-level response.

Based on changes of the activity data caused due to the lowered human activity, we estimated the emissions changes, as shown in Table 3.

3.5. Quantitative estimates of the contribution of emission reductions to changes in air quality

3.5.1. Simulation of air quality changes during the COVID-19 lockdown

Changes in averaged $PM_{2.5}$ concentrations at 41 cities due to COVID-19 lockdown during Level I and Level II response period are shown in Table S6. Similar results for changes in SO_2, NO_2 and O_3 concentrations are shown in Table S7-S9. Results show that because of the restricted human activities and lowered anthropogenice emissions, $PM_{2.5}$ concentrations are reduced by 25.4% to 48.1% during Level I response period. A maximum reduction of $PM_{2.5}$ concentration by 27.3 $\mu g\ m^{-3}$ is found for the city of Fuyang (located in northern Anhui province) during Level I response period while a maximum relative $PM_{2.5}$ reduction by 48.1% is found for the city of Taizhou (Jiangsu province). During the Level II respone period when restrictions on normal acitivites were loosened to some extent, reductions in $PM_{2.5}$ concentration due to lockdown range between 15.3% to 36.0%, which is approximately 10% lower than Level I response period. Concentrations of SO_2 and NO_2 are also lower due to reduced human activities. Averaged SO_2 and NO_2 concentrations were reduced by 17.9%to41.3% and 32.5%to70.3% during Level I response period; 12.0to27.0% and 3.3%to17.0% during Level II response period. On the contrary, average ozone concentrations generally show increasing trend due to lockdown. During Level I response period, 36 out of 41 cities show ozone increase with maximum increase by 25.9% in Shanghai Fuyang (the same city with maximum decrease of $PM_{2.5}$ concentrations). During Level II response period, 30 out of 41 cities show ozone increase with maximum increase by 16.8% in Shanghai. The increases of ozone concentrations, as opposed to derease to other pollutants, are associated with lowered NO_x emissions and thus weakened O_3 tritation by NO during lockdown. On average, averaged $PM_{2.5}$ concentrations cross the YRD region reduced by 27.6% and 19.4% due to lockdown during Level I and Level II reponse periods while ozone concentrations increased by 8.3% and 2.3%.

3.5.2. Source apportionment of $PM_{2.5}$ during COVID-19 lockdown

Fig. 6 shows the contribution from eight source sectors (see definition in Table S2) plus regional transport (BC) to residual average $PM_{2.5}$ concentrations for Shanghai, Hangzhou, Nanjing and Hefei during pre-lockdown, Level I and Level II response periods of the COVID-19 scenario. For all three periods, IND is the dominant $PM_{2.5}$ contributor. During pre-lockdown period when emissions were at normal level, IND contributed 27.8% (Shanghai) to 56.8% (Nanjing) of total $PM_{2.5}$ concentrations, followed by DST (9.5% to 22.2%), RES (8.6% to 22.7%), and MOB (8.0% to 15.0%). Contribution from natural sources were negligible because of low biogenic emissions during the simulation period. During Level I response period when emissions from various activities were reduced, IND still represented the dominant $PM_{2.5}$ contributor with relative contribution of 32.2% to 61.1%. However, the absolute contribution from IND dropped from 17.1 to 34.2 $\mu g/m^3$ during pre-lockdown period to 12.6 to 21.1 $\mu g\ m^{-3}$ during Level I response period. Contribution from DST and MOB were also significantly lowered during Level I response period, with relative contribution of 2.6% to 7.7% and 3.9% to 8.1%,

repectively, due to restricted construction and travelling. In contrast, relative contribution from residential sources (RES) are higher during lockdown periods (12.1% to 28.1% for Level I and 13.7% to 28.5% for Level II), exceeding contributions from MOB and DST.

Fig. 7 shows the contributions from four major source sectors to $PM_{2.5}$ during the three stages over the YRD region. As shown in the figure, industry and residential contributions to $PM_{2.5}$ is significant, while mobile source contribution is most obvious during pre-lockdown. These results indicate that re-organisation of the industrial structure, transportation structure is urgently necessary to improve future air quality.

4. Conclusions

During the COVID-19 control period, human activities have been lowered greatly, causing significant reductions in industrial operations, VKT, constructions and other activities which further leads to emissions reduction. During the most stringent Level I response period, the primary pollutants like SO_2, NO_x, $PM_{2.5}$ and VOCs have been reduced by 26%, 47%, 46% and 57%, this caused a decrease of $PM_{2.5}$ concentrations by 25.4% to 48.1% over the YRD region. However, the daily $PM_{2.5}$ still ranges between 15 and 79 $\mu g\ m^{-3}$ during the lockdown period, and O_3 rebounded by 20.5% simultaneously. Source apportionment results show that $PM_{2.5}$ during lockdown periods mainly comes from industry and residential sources. This indicates that the co-control of $PM_{2.5}$ and O_3 is quite challenging, more stringent measures like adjustment of enrgy structure and industrial structure, more stringent regional joint-control within YRD and even between YRD and northern China areas should be pushed forward to achive a better air quality.

Declaration of competing interest

The authors declare that they have no known competing financial interests or personal relationships that could have appeared to influence the work reported in this paper.

Appendix A. Supplementary data

Supplementary data to this article can be found online at https://doi.org/10.1016/j.scitotenv.2020.139282.

References

Burr, M.J., Zhang, Y., 2011. Source apportionment of fine particulate matter over the Eastern U.S. part I: source sensitivity simulations using CMAQ with the Brute Force method. Atmospheric Pollution Research 2, 300–317. https://doi.org/10.5094/apr.2011.036.

Chang, J.S., Brost, R.A., Isaksen, I.S.A., Madronich, S., Middleton, P., Stockwell, W.R., et al., 1987. A 3- dimensional eulerian acid deposition model physical concepts and formulation. J. Geophys. Res.-Atmos. 92, 14681–14700. https://doi.org/10.1029/JD092iD12p14681.

Chou, M.D., Lee, K.T., Tsay, S.C., Fu, Q., 1999. Parameterization for cloud longwave scattering for use in atmospheric models. J. Clim. 12, 159–169. https://doi.org/10.1175/1520-0442-12.1.159.

Duan, S.-G., Jiang, N., Yang, L.-M., Zhang, R.-Q., 2019. Transport pathways and potential sources of $PM_{2.5}$ during the winter in Zhengzhou. Environmental Science 40, 86–93. https://doi.org/10.13227/j.hjkx.201805187.

Ek, M.B., Mitchell, K.E., Lin, Y., Rogers, E., Grunmann, P., Koren, V., et al., 2003. Implementation of Noah land surface model advances in the National Centers for Environmental Prediction operational mesoscale ETA model. J. Geophys. Res.-Atmos. 108, 16. https://doi.org/10.1029/2002jd003296.

Hong, S.-Y., Noh, Y., Dudhia, J., 2006. A new vertical diffusion package with an explicit treatment of entrainment processes. Mon. Weather Rev. 134, 2318–2341. https://doi.org/10.1175/mwr3199.1.

Hopke, P.K., Zeng, Y., 1989. A study of the sources of acid precipitation in Ontario, Canada. Atmos. Environ. 23, 1499–1509. https://doi.org/10.1016/0004-6981(89)90409-5.

Huang, L., An, J., Koo, B., Yarwood, G., Yan, R., Wang, Y., et al., 2019. Sulfate formation during heavy winter haze events and the potential contribution from heterogeneous SO_2 + NO_2 reactions in the Yangtze River Delta region, China. Atmos. Chem. Phys. 19, 14311–14328. https://doi.org/10.5194/acp-19-14311-2019.

Li, L., An, J., Zhou, M., Qiao, L., Zhu, S., Yang, R., et al., 2018. An integrated source apportionment methodology and its application over the Yangtze River Delta Region, China. Environmental Science & Technology 52, 14216–14227. https://doi.org/10.1021/acs.est.8b01211.

Li, L., Zhu, S., An, J., Zhou, M., Wang, H., Yan, R., et al., 2019. Evaluation of the effect of regional joint-control measures on changing photochemical transformation: a comprehensive study of the optimization scenario analysis. Atmos. Chem. Phys. 19, 9037–9060. https://doi.org/10.5194/acp-19-9037-2019.

Li, M., Zhang, Q., Kurokawa, J-i., Woo, J.-H., He, K., Lu, Z., et al., 2017. MIX: a mosaic Asian anthropogenic emission inventory under the international collaboration framework of the MICS-Asia and HTAP. Atmos. Chem. Phys. 17, 935–963. https://doi.org/10.5194/acp-17-935-2017.

Lin, Y.-L., Farley, R.D., Orville, H.D., 1983. Bulk parameterization of the snow field in a cloud model. J. Clim. Appl. Meteorol. 22, 1065–1092. https://doi.org/10.1175/1520-0450(1983)022<1065:bpotsf>2.0.co;2.

Liu, T., Wang, X.-J., Chen, Q., Wen, J., Huang, B., Zhu, H.-X., et al., 2019. Pollution characteristics and source apportionment of ambient $PM_{2.5}$ during four seasons in Yantai City. Environmental Science 40, 1082–1090. https://doi.org/10.13227/j.hjkx.201807252.

Mlawer, E.J., Taubman, S.J., Brown, P.D., Iacono, M.J., Clough, S.A., 1997. Radiative transfer for inhomogeneous atmospheres: RRTM, a validated correlated-k model for the longwave. J. Geophys. Res.-Atmos. 102, 16663–16682. https://doi.org/10.1029/97jd00237.

NASA, 2020. The Earth Observatory. Retrieved from https://earthobservatory.nasa.gov/images/146362/airborne-nitrogen-dioxide-plummets-over-china.

Polissar, A.V., Hopke, P.K., Paatero, P., Kaufmann, Y.J., Hall, D.K., Bodhaine, B.A., et al., 1999. The aerosol at Barrow, Alaska: long-term trends and source locations. Atmos. Environ. 33, 2441–2458. https://doi.org/10.1016/s1352-2310(98)00423-3.

Tian, H., Liu, Y., Li, Y., Wu, C.-H., Chen, B., Kraemer, M.U.G., et al., 2020. An investigation of transmission control measures during the first 50 days of the COVID-19 epidemic in China. Science (New York, N.Y.) https://doi.org/10.1126/science.abb6105.

Wang, C., Horby, P.W., Hayden, F.G., Gao, G.F., 2020a. A novel coronavirus outbreak of global health concern. Lancet 395, 470–473. https://doi.org/10.1016/s0140-6736(20)30185-9.

Wang, P., Chen, K., Zhu, S., Wang, P., Zhang, H., 2020b. Severe air pollution events not avoided by reduced anthropogenic activities during COVID-19 outbreak. Resour. Conserv. Recycl. 158, 104814. https://doi.org/10.1016/j.resconrec.2020.104814.

Yarwood, G., et al., 2010. Updates to the carbon bond mechanism for version 6(CB6). Presented at the 9th Annual CMAS Conference, Chapel Hill, October.

Zhang, H.-Y., Cheng, S.-Y., Yao, S., Wang, X.-Q., Zhang, J.-F., 2019. Pollution characteristics and regional transport of atmospheric particulate matter in Beijing from October to November, 2016. Environmental Science 40, 1999–2009. https://doi.org/10.13227/j.hjkx.201810228.